Revision 1

Micro and nano-characterization of Zn-clays in nonsulfide supergene ores of southern Peru

Nicola Mondillo[a], Fernando Nieto[b], Giuseppina Balassone[a]

[a] *Dipartimento di Scienze della Terra, dell'Ambiente e delle Risorse, Università di Napoli Federico II, Via Mezzocannone, 8 I-80134 Napoli Italy;* nicola.mondillo@unina.it, balasson@unina.it

[b] *Departamento de Mineralogía y Petrología and IACT, Universidad de Granada, CSIC, Av. Fuentenueva, 18002 Granada, Spain;* nieto@urg.es

ABSTRACT

Zn-clays are associated with several supergene nonsulfide ore deposits worldwide, where they are either the prevailing economic minerals, or minor components of the weathering-derived mineral assemblage. A TEM-HRTEM study on Zn-clays from nonsulfide ore deposits of Accha and Yanque (Peru) was carried out, to properly specify the chemistry and complex texture of these clays, not fully determined in other previous works on these (but also on other similar) deposits. The Zn-clays occurring at Accha and Yanque are constituted by a mixture of sauconite and Zn-bearing beidellite. Here we report the first worldwide occurrence of Zn-bearing dioctahedral smectite (beidellite). Chemical formulas of sauconite and beidellite have been also established. The chemical composition of sauconite varies in a range of values, without any chemical gap, around the average composition:

$$Ca_{0.15}K_{0.05}(Zn_{2.1}Mg_{0.2}Al_{0.4}Fe_{0.15}Mn_{0.02})(Si_{3.5},Al_{0.5})O_{10}(OH)_2{\cdot}nH_2O.$$

Beidellites present a composition close to stoichiometry with the addition of Zn:

$$Ca_{0.05}K_{0.15}(Al_{1.6}Zn_{0.25}Mg_{0.1}Fe_{0.15})(Si_{3.6}Al_{0.4})O_{10}(OH)_2{\cdot}nH_2O.$$

The chemical composition of both sauconite and beidellite is consistent through the samples, with sauconite affected by a wider variation in composition than beidellite. The textures of Zn-bearing smectites clearly indicate that a part of these clays grew on precursory mica-like phyllosilicates, whereas another part was derived from a direct precipitation from solutions. The occurrence of a paragenesis with trioctahedral and dioctahedral smectites demonstrates that, as observed in other environments, also in a Zn-bearing system both smectite types are stable. As proved for other analogous trioctahedral-dioctahedral smectite systems (e.g. saponite-beidellite), also in the sauconite-beidellite system a chemical compositional gap exists within the series. The texture indicating a direct precipitation from solutions does not exclude that a smectite amount could be genetically related to hydrothermal fluids, even if several other characteristics (e.g. the paragenetical association with Fe-hydroxides typical of gossans) confirm the supergene origin for the bulk of the deposit.

Keywords: Sauconite, Zn-beidellite, nonsulfide zinc ore deposits, TEM-HRTEM

INTRODUCTION

Zn-bearing clay minerals occur in several nonsulfide zinc ores (Hitzman et al. 2003; Large 2001). Zinc nonsulfide deposits are concentrations of economic Zn-oxidized minerals, mainly represented by smithsonite, hydrozincite, hemimorphite, sauconite and willemite, markedly different from sphalerite ores, typically exploited for zinc (Hitzman et al. 2003; Large 2001). Nonsulfide ores are genetically related to supergene or hypogene processes: the supergene deposits primarily form from the oxidation of sulfide-bearing concentrations in a weathering regime, whereas the hypogene deposits form after mineral precipitation from hydrothermal or metamorphic fluids (Hitzman et al. 2003).

Zn-clays are worldwide associated with several supergene nonsulfide ores, where they are either the prevailing economic minerals, or minor components of the weathering-derived mineral assemblage (Balassone et al. 2008; Boland et al. 2003; Boni et al. 2009; Borg et al. 2003; Coppola et al. 2008; Emselle et al. 2005; Frondel 1972; Ahn 2010; Kärner 2006). The best example is the world-class Skorpion mineralization (Namibia) - the largest supergene nonsulfide zinc deposit in the world (original reserves of 24.6 Mt ore at 10.6% Zn) - where sauconite, the trioctahedral Zn-bearing smectite (Newman and Brown 1987; Ross 1946), predominates over the other Zn-oxidized minerals (Borg et al. 2003; Kärner 2006).

Herein we present the first combined TEM-AEM and HRTEM crystal-chemical characterization of natural Zn-clay minerals, associated with two nonsulfide ore deposits in Peru (Yanque and Accha). Standard EPMA and/or SEM-EDS techniques have generally not allowed to properly specifying their chemistry and complex texture, due to the tiny size of clay minerals. By contrast, TEM is pivotal for the characterization of crystalline materials at nano- and sub-nanometer scale, as clays (Nieto and Livi 2013), allowing a wide range of imaging and diffraction techniques. When coupled with AEM analytical tools, elemental composition and atomic structure down to a single atom can be provided as well. The aim of this work is to shed new light on the characteristics of the Zn-clays, which is an important issue in order to plan a correct metallurgical processing, and to better constrain their genesis.

AN OVERVIEW ON Zn-BEARING PHYLLOSILICATES

A list of Zn-bearing clay minerals and other phyllosilicates is given in Table 1. Sauconite is the predominant Zn-bearing clay in zinciferous nonsulfide ore deposits (Boni 2005; Hitzman et al. 2003). It was recognized for the first time in the Uberroth Mine, near Friendensville, in the Saucon Valley of

Pennsylvania (Genth 1875). The validity of the species was later proved by Ross (1946), who produced also the chemical formula still accepted by the International Mineralogical Association (IMA). Sauconite has a saponite-like structure, with a tetrahedral charge related to Al/Si substitutions in tetrahedral sheets (Faust 1951; Ross 1946), while Zn takes the place of Mg in the octahedral positions.

Several experimental studies on the synthesis and stability of sauconite were carried out (Harder 1977; Higashi et al. 2002; Kloprogge et al. 1999; Pascua et al. 2010; Petit et al. 2008; Roy and Mumpton 1956; Tiller and Pickering 1974). These studies demonstrated that Zn-smectite can precipitate from solutions of silicic acid, variously mixed with Zn-compounds (Zn-chloride, Zn-oxide or Zn-hydroxide), Na-compounds and Al-compounds, at temperatures ranging between 20° and 200°C for pH from 6 to 12. The retention of base (Zn) and heavy metals in other phyllosilicate lattices through adsorption mechanisms, as in kaolinite, has been also investigated (Gu and Evans 2008; Miranda-Trevino and Coles 2003; Srivastava et al. 2005).

Several occurrences of sauconite have been reported worldwide, e.g. in the Moresnet-Altenberg nonsulfide deposit (La Calamine) in Belgium (Coppola et al. 2008; Frondel 1972), in the supergene weathering zones of the Irish Tynagh and Silvermines deposits (Balassone et al. 2008), in the Shaimerden deposit, Kazakhstan (Boland et al. 2003), in the Sierra Mojada Zn district in Mexico (Ahn 2010), and in the Reliance deposit near Beltana, South Australia (Emselle et al. 2005; Hitzman et al. 2003). In these deposits, sauconite is associated with smithsonite and hemimorphite, and is considered a product of the weathering of Zn-bearing sulfides. In the Skorpion zinc deposit (Namibia), sauconite mainly occurs as coatings of intergranular spaces and voids; it formed after the breakdown and dissolution of feldspars and micas (Borg et al. 2003; Kärner 2006).

All the other Zn-bearing phyllosilicates have been generally considered as rare species in natural Zn-oxidized deposits (Hitzman et al. 2003).

Fraipontite, a Zn-bearing clay belonging to the kaolinite-serpentine group, was first described by

Cesàro (1927), who found a "*silicate double de zinc et d'aluminium hydraté*" in the Vieille-Montagne Mine (Belgium). The mineral was definitely validated by Fransolet and Bourguignon (1975), who carried out a structural characterization of the original specimen and also proposed the chemical formula actually accepted by IMA. Fraipontite is considered a weathering-related clay mineral, as, for example, in the Belgian deposits (Coppola et al. 2008), or also associated with low-temperature hydrothermal fluids, as in Preguic□a mine, Southern Portugal (Will et al., 2014).

Baileychlore, the Zn-bearing end-member of the trioctahedral chlorite series, was recognized and validated by Rule and Radke (1988) in a specimen from the Red Dome deposit, North Queensland (Australia).

A Zn-phyllosilicate intermediate between chlorite and mica is the franklinfurnaceite (Peacor et al. 1988), which was solely recognized in association with willemite in the Franklin mine, New Jersey (USA).

Up to date, in clearly hydrothermal/metamorphic deposits in USA (e.g., Franklin, New Yersey) and Australia (Broken Hill), two types of Zn-mica have been identified, i.e. bannisterite (Heaney et al. 1992) and hendricksite (Robert and Gaspérin 1985).

BACKGROUND INFORMATION ON PERUVIAN Zn CLAY-BEARING DEPOSITS

Geological setting

The present study is based on the Zn-smectites from the Yanque and Accha nonsulfide Zn-Pb deposits, Cuzco region, in southern Peru (Boni et al. 2009; Mondillo et al. 2014a).

The Yanque and Accha deposits are located in the Andahuaylas-Yauri metallogenic province, extending for several hundred square kilometers around the town of Cuzco. The Andahuaylas-Yauri

province hosts numerous porphyry copper and porphyry-related skarn deposits that are spatially and temporally associated with the middle Eocene to early Oligocene (ca. 48-32 Ma) intrusions of the Andahuaylas-Yauri batholith into Mesozoic sediments (Fig. 1a) (Perelló et al. 2003). The Accha-Yanque Belt covers a wide area located in the middle of the Andahuaylas province; it hosts many Zn and Pb ores, as well as several porphyry copper deposits of variable sizes.

The Yanque prospect is a Zn-Pb nonsulfide concentration located 20 km north of Santo Tomás village. The orebody covers an approximate surface area of 900 by 500 m, and contains 26,491 kilotonnes of indicated resources at 2.37% Zn and 2.18% Pb (1.67% ZnEq cutoff) (Zincore Metals, Inc., 2013). The deposit consists of several sub-horizontal stratabound bodies that extend in depth to more than 100 m. Yanque is hosted by a sedimentary breccia with lateral facies variations, which stratigraphically comprehends parts of the Mara and Ferrobamba Formations (Pecho and Blanco 1983) (Fig. 1b). The mineralized breccia consists of a siliciclastic conglomerate, heteropic to a breccia containing dolomite clasts. This sedimentary breccia was affected by phyllic alteration, with alteration of feldspars and precipitation of microcrystalline mica, related to the emplacement of the original sulfide mineralization (Mondillo et al. 2014a).

The Accha deposit is a sphalerite mineralization hosted in Mesozoic rocks, almost fully oxidized to smithsonite. The mineralized zone [6,613 kilotonnes of measured and indicated resources at 6.37% Zn and 0.78% Pb (2.20% ZnEq cutoff) (Zincore Metals, Inc. 2013)] occupies the hinge of an anticlinal dome that has been exposed by erosion. The nonsulfide concentrations, consisting of a mineralized zone 5 to 20 m thick, are continuous along strike to the west for at least 700 m (Boni et al. 2009).

The main host to mineralization consists of carbonate-clay matrix-supported breccias and locally by very thin, quartz-rich conglomerate layers (Fig. 1c). The total thickness of the brecciated interval, visible both in outcrop and in drill core, varies from 50 to 100 m, whereas individual breccia zones are continuous over 5 to 20 m downhole (Boni et al. 2009).

Both Yanque and Accha nonsulfide deposits formed after the oxidation of original sulfide protores, which, together with several Cu-porphyry deposits, are genetically related to the emplacement of the Andahuaylas-Yauri batholith (Boni et al. 2009; Mondillo et al. 2014a, b).

Mineralogy and petrography of Yanque and Accha ores

Sauconite is the most abundant economic Zn mineral in the Yanque deposit (Mondillo et al. 2014a). It was observed in association with a Zn-bearing mica (indicated as Zn-illite by the above authors) with Zn in its octahedral site, and with a Zn-bearing kaolinite, where Zn was considered not to be a cation in the clay structure, but an element adsorbed by the Fe-hydroxides associated with clays (Mondillo et al. 2014a). Sauconite in the Yanque deposit was considered to have been mainly formed through replacement of K-feldspar and muscovite of the host rock by weathering process. Other components of the Yanque mineralization are hemimorphite, smithsonite, cerussite and secondary silver sulfides (i.e. acanthite). The original primary sulfides are virtually lacking in the deposit.

The Accha nonsulfide mineral association consists mainly of smithsonite and hemimorphite replacing both primary ore minerals and carbonate host rocks. Sauconite is less abundant, but it has been detected throughout the deposit with the more abundant smithsonite and hemimorphite. According to Boni et al. (2009) sauconite is genetically related to supergene transformation of the potassic alumosilicates, and/or forms the filling of the remaining porosity of the host rock.

X-ray diffraction analyses were carried out on clay separates of Yanque samples by Mondillo et al. (2014a) under different conditions. X-ray diffraction patterns of the air-dried, ethylene glycol solvated, and heated (550°C) clay aggregates resulted to be typical of expandable smectites, here identified as sauconite (Table 2). These analyses allowed excluding the occurrence in the Yanque deposit of Zn-bearing phyllosilicates of the chlorite group (e.g. baileychlore), which have almost the same air-dried pattern of sauconite, but are characterized by non-expandable characteristics.

MATERIALS

For TEM-AEM analyses, we have selected five samples from the Yanque deposit and one sample from the Accha deposit, by using drillcore sections having medium-high Zn-grade and moderate/high clay contents, already analyzed by Boni et al. (2009) and Mondillo et al. (2014a). Their mineral assemblages, inferred by semi-quantitative mineralogical X-ray diffraction, are reported in Table 2.

Yanque samples are characterized by abundant phyllosilicates, in particular sauconite, illite and kaolinite (Table 2). Samples YA-D, and YA-E originate from some deeply altered parts of the siliciclastic conglomerate which hosts the Yanque Zn-Pb mineralization, whereas samples YA-A, YA-B, and YA-C were collected from sandstone-shale lenses within the conglomerate.

Sample ACC was collected in the Accha deposit from a mineralized quartz-rich conglomerate layer with abundant sauconite, interlayered within the limestone containing the main smithsonite orebody. This sample mostly consists of detrital quartz, Zn-Mn-hydroxides (mostly chalcophanite) and sauconite (Table 2).

METHODS

The particle morphology and quantitative chemical analyses were obtained using TEM and AEM respectively. The microscope used was a Philips CM20, at the C.I.C. of the University of Granada, operating at 200 kV, with an EDAX solid state EDX detector. Lifetime of analyses was 100 seconds; areas producing dead time higher than 5% were rejected to ensure the thin character required by the Cliff and Lorimer (1975) approximation. Analyses were obtained, using STEM mode, from powdered

193 portions deposited on a holey C-coated Au grid. This mode of preparation disperses individual grains
194 of minerals onto the grid surface. Albite, biotite, muscovite, spessartine, olivine, titanite and
195 hemimorphite standards were measured using the same protocol as samples, to obtain K-factors for the
196 transformation of intensity ratios to concentration ratios according to Cliff and Lorimer (1975). The
197 structural formulae of smectite and mica were calculated on the basis of 22 negative charges, i.e.
198 $O_{10}(OH)_2$. According to the accepted stoichiometry of smectites (Güven, 1988), Fe was considered as
199 bivalent for trioctahedral species (e.g. sauconite), and trivalent for dioctahedral species (e.g. beidellite).
200 The Na content in the Zn-clays was not measured, because of the Na-Zn peaks overlap in the energy
201 dispersion spectrum. However, as reported by Mondillo et al. (2014a), ICP-MS analyses on a clay-rich
202 fraction excluded the occurrence of significant amounts of Na in these minerals, where a maximum
203 content of about 0.5 % of this element has been detected.
204 Two samples (YA-B and YA-D) were also analyzed in HRTEM mode on thin sections, in order to
205 investigate the microscopic texture of clays. The samples were chosen considering their different clay
206 association detected at TEM-AEM. Copper rings were attached to representative selected areas of the
207 matrix of thin sections prepared with Canada balsam and after ion-thinned, using a Fischione Model
208 1050 ion mill, and carbon coated. Ion milling was performed at 4 Kv and ±10º, until the first hole and
209 ±7º during 20 minutes for final cleaning. The HRTEM study was performed at the CIC of the
210 University of Granada (Spain) using a Titan TEM with XFEG emission gun, spherical aberration
211 corrector and HAADF detector, working at 300 kV, with a resolution of 0.8 Å in the TEM mode and 2
212 Å in the STEM mode. EDX spectra for qualitative identification of minerals and chemical maps were
213 obtained using the Super-X system.
214
215
216 **RESULTS**

Texture of clays

The texture of the Zn-clays was observed in the samples YA-B and YA-D, whose preparation using ion-milling technique provided the preservation of the mineral fabric (Fig. 2 and 3). At low magnification, the two samples present similar characteristics, and they generally produce comparable electron diffraction patterns (SAED). Therefore they will be described together.

At a size below 10 μm, smectite forms two types of microtextures here indicated as "compact clay packages" (CCP) and "porous clay aggregates" (PCA) (Fig. 2a, b).

CCP (Fig. 2a) are characterized by nearly isoriented clay packets. This microtexture can have a length up to several micrometers and a thickness below 1 μm, and the packets can be straight or slightly curved. In the packets, the clay layers can be curved and show a wavy microfabric. In the CCP, smectite grains can overgrow upon mica nuclei, forming a sort of epitaxial structure (Fig. 2c, d). Compact smectite packets produce electron diffraction patterns constituted by the superposition of concentric circles, characteristic of a powder-type diagram, and oblique trends of points, corresponding to various individual crystals partly disoriented between each other (Fig. 4). Both the powder circles and mono-crystals have a 10 Å spacing, which indicates the typical collapse of smectitic layers related to the microscope vacuum. Figure 4b shows the electron diffraction pattern of the smectite packet shown on figures 2c and d, epitaxial over a mica grain; both smectite and mica present a 10 Å basal spacing, but they can be easily distinguished by their different crystallinity. Mica electron diffraction pattern shows also some general rows having a spacing of 20 Å, which allows the identification of mica 2M polytype.

The PCA are characterized by random orientation of the clay packets, which typically show a very fine grain size, lower than those detected in CCP (Fig. 2b). The random orientation produces radial to dendritic microtextures and leaves spaces between the grains. The voids of these aggregates are

241 frequently occupied by Fe-hydroxides (Fig. 2e, f, Fig. 3), which can have a spongy texture (Fig. 2e), or
242 also occur as rhombic micro-grains and radial aggregates of oblong crystals (Fig. 2f). Electron
243 diffraction patterns of PCA show that smectite has a turbostratic arrangement. When the porous packets
244 are associated with Fe-hydroxides, the electron diffraction pattern shows the superposition of the
245 smectite and the Fe-hydroxides patterns. Fe-hydroxides pattern is compatible with crystal structure
246 characteristics of goethite.
247 As reported in previous studies (Amouric and Olives 1998; Cuadros et al. 2009), it is difficult to obtain
248 lattice-fringe HRTEM images from very hydrated clays, as smectites, because of the structural damage
249 caused by the electron beam. Another problem is related to the vacuum of the TEM environment and/or
250 electron irradiation, which cause dehydratation and collapse of smectite. It results that the usually
251 measured smectite spacing is 10 Å in the case of a complete collapse, or >10 Å in case of an
252 incomplete collapse.
253 At high resolution, the samples generally show smectite packets with lattice fringes whose spacing
254 ranges from 10 to 11 Å (Fig. 5a), but notable differences have been also revealed. For example, Figure
255 5b presents lattice fringes, which show random interstratification of smectite and mica with measured
256 spacing of 20 Å. This random smectite/mica interstratification has been recognized by the electron
257 diffraction pattern, where it was possible to measure a non-rational order of very diffuse basal
258 reflections with calculated spacing of 11.2 Å, from the (001) spot, 9.8 and 8.9 Å from (002), and 9.8 Å
259 as of (003). Moreover, the EDX spectra of these areas showed an intermediate composition between
260 those usually found for sauconite and mica. In the same figure (Fig. 5b) a fringe spacing of 18 Å was
261 also measured. Somewhere smectite packets presenting alternating fringes at 13 and 10 Å were
262 detected (Fig. 5c). In a two-dimensional lattice image (Fig. 5d) of a smectite packet characterized by
263 lattice fringes with spacing of 11.6 Å, it is possible to recognize crystallographic coherence from layer
264 to layer and that the 11.6 Å spacing is the sum of 4+7.6 Å. The spacing in the perpendicular direction

is 4.5 Å, which corresponds to b/2. Figure 5e presents a smectite packet with lattice fringe spacing varying between 16 and 17 Å, and wavy microfabric. In the wavy microfabric it is possible to see coalescing and lens-like shaped sauconite packets. Other compact sauconite packets with lattice-fringe spacing of 13-15 Å and wavy microtexture, which is reflected in the curved and lens-like structure of the sauconite layers/packets, can also be recognized in the YA-B sample. Smectite layers also exhibit layer terminations. Iron hydroxide (goethite) and oxide (hematite) associated with smectite have a mosaic-domain type texture (Fig. 5f), in which the different domains present variable orientation and spacing.

It was possible to carry out qualitative chemical analyses (EDX spectra) of particles during the observation, with the Titan TEM used for the textural analysis. In this way, together with textural information, it was possible to obtain data on crystal structure and chemistry of phases (STEM-EDX). It was revealed that in both CCP and PCA, smectite occurs in the two species, sauconite and beidellite, identified in the Titan by their qualitative chemical differences (Fig. 6). In fact, the Zn and Al contents of the two kinds of smectites are so different that qualitative differentiation is straightforward.

Chemical composition of Zn-clays by TEM-AEM

Considering that AEM is not an absolute-composition technique, and allows determining only the ratios between the various elements, it is usually required to normalize the obtained chemical compositions to the basic formula of the investigated minerals.

From the analyses of the dispersed mineral grains in the samples, it was ascertained that Yanque smectite is mostly composed by sauconite; it is associated with a discrete amount of Zn-bearing beidellite and few grains of illite. Beidellite was detected in all the Yanque samples, but only in YA-A, YA-B, and YA-E proper contamination-free quantitative chemical compositions could be obtained.

In the Accha sample, similarly to Yanque, sauconite is the most abundant clay mineral. Few beidellite

289 and/or montmorillonite grains were also detected, but here they were found intimately associated with
290 sauconite. Consequently, as in some Yanque samples, it was not possible to obtain acceptable
291 contamination-free quantitative chemical composition of this beidellite; however a montmorillonite
292 grain could be analyzed.
293 In Tables 3 and 4, we report some representative chemical compositions of Zn-clays from the Yanque
294 and Accha samples, normalized to $O_{10}(OH)_2$. The octahedral sites are occupied by Zn, Mg, Mn, Fe, and
295 Al cations, whereas K and Ca were considered as interlayer cations.
296 Sauconite is characterized by a variable composition (Table 3), which could be, in a minor extent, a
297 consequence of the minor presence of interstratifications with mica layers as shown in Fig. 5b. Silicon
298 can fully occupy the tetrahedral site or decrease continuously up to 3.27 a.p.f.u. (atoms per formula
299 units) (Fig. 7a), with the remaining amount compensated by Al^{IV} (Fig. 7b). The comparison between
300 Accha and Yanque samples shows that Accha sauconite seems to be characterized by an Al^{IV} amount
301 ($0.5 < Al^{IV} < 0.8$ a.p.f.u) higher than Yanque one ($0.1 < Al^{IV} < 0.7$ a.p.f.u.) (Fig. 7b).
302 In both the Accha and Yanque samples, sauconite octahedral composition remains coherent through the
303 data (Figs. 7 and 8). Most of the octahedral site is occupied by Zn, which has been found to completely
304 fill the site only in one case (3 atoms per formula units, a.p.f.u.) (Fig. 7c); it generally varies
305 continuously between 2.66 a.p.f.u and 1.67 a.p.f.u., and only in three grains comes down to 1.40 a.p.f.u.
306 The octahedral site can be also occupied by Al (0.13–0.72 a.p.f.u.) (Fig. 7c), Mg (up to 0.46 a.p.f.u.,
307 generally lower than 0.30 a.p.f.u.) (Fig. 7d), Fe (up to 0.57 a.p.f.u., generally below 0.40 a.p.f.u.) (Fig.
308 7e), and Mn (between 0.04 and 0.48 a.p.f.u. in a few grains, but generally below detection limits). As
309 regards the measured octahedral Fe, sauconite is often intergrown with Fe-hydroxides and oxides:
310 consequently the iron content could be enhanced by the contribution of oxyhydroxides-related Fe in
311 some analytical points.
312 Plotting Zn/Al_{tot} vs. Si/Al_{tot} a positive correlation is observed, with ratio values ranging from 1 to 5 for

313 Zn/Al_{tot} and from 2 to 10 for Si/Al_{tot} (Fig. 7f).

314 The interlayer content is represented by K and Ca occurring in variable amounts, within the ranges of
315 0.00–0.27 a.p.f.u. and 0.00–0.38 a.p.f.u. for K and Ca, respectively (Fig. 7g, h). Calcium is more
316 abundant than K, with the values of the latter generally approaching zero. K and Ca are positively
317 correlated (Fig. 7h), and Ca/K ratio ranges between 1 and 8. The Accha sauconite contains Ca amounts
318 slightly higher than Yanque sauconite, as a result of the charge compensation related to the different
319 Al^{IV} content (Fig. 7b, h). As previously discussed, Na cannot be revealed in the presence of Zn by
320 TEM-AEM, and hence has not considered as interlayer cation.

321 Correlation of Zn/Al_{tot} *vs* Ca/K ratios generally show a positive trend, which is coherent with charge
322 compensation between the layers (Fig. 7i).

323 As regards beidellite, the following data are associated with Yanque samples: beidellite was detected
324 by AEM analysis in few areas (Table 4), and shows a tetrahedral occupancy very similar to sauconite,
325 with Si in the range of 3.36–3.83 a.p.f.u. (Fig. 7a). The octahedral Al generally varies between 1.29
326 a.p.f.u. and the maximum stoichiometric value of 2 a.p.f.u. (measured only in two grains). In the Zn-
327 bearing beidellites, Zn varies between 0.14 and 0.54 a.p.f.u. (Fig. 7c). As in sauconite, the other
328 octahedral cations show low values: Mg varies between 0.00–0.31 a.p.f.u. (Fig. 7d), Fe ranges between
329 0.00–0.38 a.p.f.u. (Fig. 7e), whereas Mn is lacking, except for 0.02 a.p.f.u. detected only in one Zn-
330 beidellite grain. The Zn/Al_{tot} and Si/Al_{tot} ratios vary for a very short range of values (Zn/Al_{tot} between
331 0–0.25; Si/Al^{tot} between 1.27–2.31) and no correlations were observed (Fig. 7f). Zn vs. Al^{VI} plot (Fig.
332 7c) shows that the distribution of the two elements is clearly related to their charge, with divalent Zn
333 reaching a maximum occupancy of 3 a.p.f.u. in sauconite, whereas trivalent Al reaches a maximum
334 occupancy of 2 a.p.f.u. in beidellite.

335 In dioctahedral clay minerals, the interlayer cations are K and Ca, as already discussed for sauconite,
336 but in beidellite K (max. 0.17 a.p.f.u.) is prevailing compared to Ca (max. 0.14 a.p.f.u.) (Fig. 7h). The

K and Ca contents are positively correlated, but the Ca/K statistic ratio is around 1.2, with absolute ratios ranging between 0 and 1.5 (Fig. 7h). This correlation, more favorable to K than Ca is in agreement with the charge compensation principle and the higher Al^{3+} content in beidellite than in sauconite. Smectites can have some Mg amounts in the interlayer; however, no definitive criteria exist on Mg distribution between the octahedral sheet and the interlayer. Some formulae showing high-octahedral and/or low-interlayer sums could be better adjusted considering part of Mg as an interlayer cation, which could explain such anomalies. Nevertheless, we have accepted such possibility only for straightforward cases as those of the beidellites in sample YA-E (Table 4).

The other detected clays also show discrete Zn contents. Montmorillonite is characterized by an octahedral occupancy almost equally subdivided between Al and Mg-Zn, which have amounts of 1.06 a.p.f.u. Al, 0.55 a.p.f.u. Mg, and 0.39 a.p.f.u. Zn. An illite grain with interlayer cationic content of ~0.55 a.p.f.u. is characterized by 0.04 a.p.f.u. Zn in the octahedral site. Chemical analysis of micas was not considered to be an objective during AEM data acquisition; hence the micas were not systematically analyzed. However, several micas completely free of Zn were found during the HRTEM analysis (e.g. see figures 2c and 2d), together with others with a minor Zn content.

DISCUSSION

This TEM-HRTEM study carried out on natural Zn-smectites allowed to obtain new results mainly focused on the very detailed identification of the clay type, on the mineral texture, and chemical composition.

Clay type identification

Our results have shown that the Zn-bearing clay fraction of the Accha and Yanque supergene ores, previously simply identified as sauconite (Accha) or sauconite+Zn-bearing illite+kaolinite (Yanque), is indeed a mixture of several smectites, i.e. the trioctahedral sauconite and the dioctahedral (both Zn-bearing and Zn-poor) beidellite. The occurrence of a Zn-bearing beidellite was never ascertained, either in nonsulfide Zn deposits and worldwide.

In our opinion, the misinterpretation of the nature of the clay minerals, made in the previous studies is due to the use of protocols of combined XRD and EPMA, routinely applied to the mineralogical evaluation of the ores, on the basis of the previous literature on this type of deposits. Specifically, bulk rock XRD analyses allowed to basically identifying the occurrence of smectite in the Accha deposit, and of smectite, mica (illite), and kaolinite in the Yanque deposit. When a combination of microbeam analyses as EPMA-EDS was employed, the numerous textural and petrographic observations led to automatically consider all the Zn-Al-Si-H_2O analyses as sauconite, the K-Al-Si-H_2O-(few Zn) analyses as Zn-bearing illite, and Al-Si-H_2O-(few Zn) analyses as Zn-bearing kaolinite. The TEM-STEM-HRTEM technique enabled instead to test every chemical STEM analysis, by using electron diffraction and lattice images, and allowed to confirm in the studied samples the occurrence of sauconite and of a Zn-bearing mica (not deeply investigated in this study). It also evidenced that the analyses containing Al-Si-H_2O-(few Zn) were not corresponding to a Zn-bearing kaolinite, but again to a smectite and specifically to a Zn-bearing beidellite. In our opinion, it could be possible that the total absence of TEM-STEM studies on natural Zn-clays (except perhaps the pioneer STEM study of Steinberg et al. 1985), favored the lack of a correct identification of other types of Zn-smectite in several ore deposits.

Texture of minerals

In the texture here called CCP, smectite frequently overgrows the mica grains. The overgrowing of CCP smectite upon mica nuclei probably indicates that the CCP inherit the crystallographic orientation

from previous phyllosilicates, which could act as templates. This is also supported by the presence of the random interstratification of smectite and mica, which has been recognized by the intermediate chemical composition, by lattice fringe images where packets showing 20 Å spacing were directly observed, and by the electron diffraction pattern. In the latter, it was possible to measure a non-rational order of basal reflections with calculated spacing of 11.2 Å to 8.9 Å.

Direct HRTEM observation of lattice fringes of the compact sauconite packets often showed a variable spacing, generally ranging around 10-11 Å, but also varying up to 13, 15 or 18 Å. We interpret these variable thicknesses of the smectite layers as possibly related to a different contracting behavior (related to TEM vacuum) of layers, in correspondence to different types of interlayer cation content (Nieto et al. 1996). An alternative explanation (especially for the 18 Å spacing) could be an interstratification, however not precisely identified during this study.

The occurrence in the CCP of coalescing packets, lens-like shaped packets, wavy microtexture, and layer terminations are features similar to those observed in other smectites of various origins (e.g. Mellini et al. 1991; Nieto et al. 1996; Vazquez et al. 2014).

The PCA textures are typical of clays directly precipitated from solutions. Consequently, they are constituted by newly formed smectite grown in the cavities existing between the CCP. Spongy or rhombic goethite and hematite occur in the PCA porosity (Fig. 3). This common textural relationship suggests that the Fe-hydroxides and oxides are syn- to post-genetic with the precipitations of clays.

Like CCP, PCA show an annular electron diffraction pattern that indicates a turbostratic disorder, typical of most smectites.

From a textural point of view, there is no difference between sauconite and beidellite, suggesting a syn-genetic origin.

Chemical composition

409 This first TEM-AEM investigation demonstrates that the chemical composition of sauconite varies in a
410 range of values, without any chemical gap, around the average composition:

411 $$Ca_{0.15}K_{0.05}(Zn_{2.1}Mg_{0.2}Al_{0.4}Fe_{0.15}Mn_{0.02})(Si_{3.5},Al_{0.5})O_{10}(OH)_2 \cdot nH_2O.$$

412 As expected, sauconite has been found to have a chemical composition characterized by Zn associated
413 with Mg, Al, Fe and Mn in the octahedral layer, a variable but significant Al tetrahedral occupancy,
414 and Ca and K as major interlayer cations.
415 The wide range of measured compositions could partially be affected also by smectite/mica
416 interstratification, clearly observed in the Yanque samples. This can likely influence Al^{IV}, Mg and
417 interlayer cation contents, and led them to vary more than expected for such type of smectite.
418 The only sauconite sample from Accha analyzed here shows a composition characterized by an average
419 Al^{IV} content slightly higher than in the above mentioned formula (Al^{IV} ~ 0.65 a.p.f.u.), and as
420 consequence of the charges compensation, also by a slightly higher interlayer Ca content (Ca ~ 0.22-
421 0.23 a.p.f.u.). Anyway, it is reasonable to suppose that this chemical feature related to just one sample
422 could not be fully representative of the whole deposit.
423 Another remarkable result of this research is that beidellite from both these Peruvian nonsulfide
424 deposits is always characterized by variable but significant Zn contents in its structure. Unfortunately,
425 the analysis of beidellites in the Accha sample has not produced acceptable results, and only data from
426 Yanque samples could be presented.
427 Beidellites have a composition close to stoichiometry with the addition of Zn:

428 $$Ca_{0.05}K_{0.15}(Al_{1.6}Zn_{0.25}Mg_{0.1}Fe_{0.15})(Si_{3.6}Al_{0.4})O_{10}(OH)_2 \cdot nH_2O.$$

429 There are various studies on beidellite containing divalent cations, and on its chemical relationship with
430 trivalent smectite end members, e.g. saponite (Grauby et al. 1993, and references therein). They
431 showed that the natural trioctahedral-dioctahedral smectite series is discontinuous with large chemical
432 gaps. From our data, a chemical gap also exists between sauconite and Zn-bearing beidellite, with an

effective maximum Al content in sauconite around 0.50 a.p.f.u. and a minimum content in beidellite around 1.30 a.p.f.u.

The Zn/Al_{tot} *vs.* Si/Al_{tot} positive correlation registered for sauconite, against the very short range of values of the same ratios of beidellites, demonstrates that the relative sauconite composition is more variable than beidellite composition in the studied samples. A consequence of the variable amount of Zn-Al in the octahedral site of sauconite and beidellite is that also the interlayer cations distribution within the clay lattice, being strictly dependent on the charge balance, vary accordingly.

IMPLICATIONS

The mineralogical study of clay minerals from Accha and Yanque nonsulfide deposits demonstrates that the mineral compounds, up to now usually called "sauconites" indeed correspond to a mixture of sauconite and Zn-bearing beidellite. This is a relevant hint, demonstrating that in such Zn-bearing systems both trioctahedral and dioctahedral smectitic structures can form, as commonly observed in Zn-free natural paragenesis of trioctahedral and dioctahedral smectites, like saponite and beidellite (e.g. Abad et al. 2003; Jiménez-Millán et al. 2008). In low-temperature environments, newly formed phases are highly dependent on the local chemistry; hence the chemical nature of each smectite grain is strongly controlled by the near particles and fluids from which it has grown (e.g. Drief at al. 2001)

The textures of the clays suggest two genetic mechanisms, i.e. smectites can grow on previous phyllosilicates (mica) (CCP texture), and/or directly precipitate from solutions (PCA texture). The first texture confirms what reported in previous studies by Boni et al. (2009) and Mondillo et al. (2014a), when the authors refer to sauconite as a "wall-rock replacement" mineral. The second PCA texture, instead, likely opens new genetic scenarios, because, as reported in literature (Roy and Mumpton 1956; Tiller and Pickering 1974; Harder 1977; Kloprogge et al. 1999; Higashi et al. 2002; Petit et al. 2008;

Pascua et al. 2010), experimental studies demonstrated that sauconite can precipitate from solutions of silicic acid, variously mixed with Zn- and other components, at temperatures ranging between 20° and 200°C for pH of 6 to 12. Consequently, it is possible to admit that PCA smectite can also form during hydrothermal processes. Considering the geological features of the deposits, their strong association with oxidized sulfides, and the link between PCA and Fe-hydroxides and oxides (typical of gossans and of weathering-related environments), we can affirm beyond doubt that most of the smectite is genetically related to supergene processes. However, at least part of it could have also been precipitated through the hydrothermal fluid circulation, which was active in the area during sulfides mineralization or slightly after their deposition, before the formation of the Fe-hydroxides and oxides typical of the gossan.

The discovery in the Peruvian nonsulfide Zn deposits of a natural association of smectites belonging to the trioctahedral sauconite and the dioctahedral (both Zn-bearing and Zn-poor) beidellite types should be considered not only a simple new mineral finding, but also an important methodological clue for future mineralogical evaluation of Zn-nonsulfide deposits with possible processing implications.

ACKNOWLEDGEMENTS

N. Mondillo thanks Prof. M. Boni for her constant support during this research. This work was partially financed by Research Projects CGL2011-30153-C02-01 and CGL2012-32169 (Spanish Ministry of Science) and the Research Group RNM-0179 of the Junta de Andalucía, and supported by the Università di Napoli grant RDIP2013 to G. Balassone.

REFERENCES

Abad, I., Jimenez-Millan, J., Molina, J.M., Nieto, F., and Vera, J.A. (2003) Anomalous reverse zoning

of saponite and corrensite caused by contact metamorphism and hydrothermal alteration of marly rocks associated with subvolcanic bodies. Clays and Clay Minerals, 51, 543–554.

Ahn, H.I. (2010) Mineralogy and geochemistry of the Non-sulfide Zn deposits in the Sierra Mojada district, Coahuila, Mexico, 193 p. Ph.D. Thesis, University of Texas, Austin, USA.

Amouric, M., and Olives, J. (1998) Transformation mechanisms and interstratification in conversion of smectite to kaolinite: an HRTEM study. Clays and Clay Minerals, 46, 521–527.

Balassone, G., Rossi, M., Boni, M., Stanley, G., and McDermott, P. (2008) Mineralogical and geochemical characterization of nonsulfide Zn-Pb mineralization at Silvermines and Galmoy (Irish Midlands). Ore Geology Reviews, 33, 168–186.

Boland, M.B., Kelly, J.G., and Schaffalitzky, C. (2003) The Shaimerden supergene zinc deposit, Kazak hstan: a preliminary examination. Economic Geology, 98, 787–795.

Boni M., Balassone G., Arseneau V., and Schmidt P. (2009) The nonsulphide zinc deposit at Accha (southern Peru): geological and mineralogical characterization. Economic Geology, 104, 267–289.

Boni, M. (2005) The geology and mineralogy of nonsulfide zinc ore deposits. Proceedings of LEAD and ZINC ’05 Congress, Kyoto, Japan, 17–19 October 2005, 15 p.

Borg, G., Kärner, K., Buxton, M., Armstrong, R., and Van Der Merwe, S.W. (2003) Geology of the Skorpion supergene zinc deposit, southern Namibia. Economic Geology, 98, 749–771.

Cesàro, G. (1927) Sur la fraipontite, silicate basique hydraté de zinc et d'aluminum. Annales Societe Geologique Belgique, 50, 106–110.

Cliff, G., and Lorimer, G.W. (1975) The quantitative analysis of thin specimens. Journal of Microscopy, 103, 203–207.

Coppola, V., Boni, M., Gilg, H.A., Balassone, G., and Dejonghe, L. (2008) The Calamine Nonsulfide Zn-Pb deposits of Belgium: petrographical, mineralogical and geochemical characterization. Ore

Geology Reviews, 33, 187–210.

Cuadros, J., Nieto, F., Wing-Dudek, T. (2009) Crystal-chemical changes of mixed-layer kaolinite-smectite with progressive kaolinization, as investigated by TEM-AEM and HRTEM. Clays and Clay Minerals, 57, 742–750.

Drief, A., Nieto, F., and Sánchez-Navas, A. (2000) Experimental clay-mineral formation from a subvolcanic rock by interaction with 1 M NaOH solution at room temperature. Clays and Clay Minerals, 49, 92–106.

Emselle, N., McPhail, D.C., and Welch, S.A. (2005) Reliance, Flinders Ranges. In Roach, I.C., Ed., Mineralogy, Geochemistry and Zinc Dispersion around a Nonsulfide Orebody, Regolith 2005 – Ten Years of CRC LEME, 86–90.

Faust, G.T. (1951) Thermal analysis and X-ray studies of sauconite and of some zinc minerals of the same paragenetic association. American Mineralogist, 36, 795–822.

Fransolet, A.M., and Bourguignon P. (1975) Données nouvelles sur la fraipontite de Moresnet (Belgique). Bulletin de la Société Française de Minéralogie, 98, 235–244.

Frondel, C. (1972) The minerals of Franklin and Sterling Hill - a checklist, 94 p. Wiley Interscience, New York.

Genth, F.A. (1875) Mineralogy of Pennsylvania. Second Geological Survey of Pennsylvania, 120 p.

Grauby, O., Petit, S., Decarreau, A., Baronnet, A. (1993) The beidellite-saponite series: an experimental approach. European Journal of Mineralogy, 5, 623–635.

Gu, X., and Evans, J. (2008) Surface complexation modeling of Cd(II), Cu(II), Ni(II), Pb(II) and Zn(II) adsorption onto kaolinite. Geochimica et Cosmochimica Acta, 72, 267–276.

Güven N. (1988) Smectite. In Bailey, S.W., Ed., Hydrous Phyllosilicates, Reviews in Mineralogy, Mineralogical Society of America, n. 19, p. 497–559, Washington D.C., USA.

Harder, H. (1977) Clay mineral formation under lateritic weathering conditions. Clay Minerals, 12,

281–288.

Heaney, P.J., Post, J.E., Evans, H.T. (1992) The crystal structure of bannisterite. Clays and Clay Minerals, 40, 129–144.

Higashi, S., Miki, K., and Komarneni, S. (2002) Hydrothermal synthesis of Zn-smectite. Clays and Clay Minerals, 50, 299–305.

Hitzman, M.W., Reynolds, N.A., Sangster, D.F., Allen, C.R., and Carman, C.E. (2003) Classification, genesis, and exploration guides for nonsulfide zinc deposits. Economic Geology, 98, 685–714.

Jiménez-Millán, J., Abad, I., and Nieto, F. (2008) Contrasting alteration processes in hydrothermally altered dolerites from the Betic Cordillera, Spain. Clay Minerals, 43, 267–280.

Kärner, K. (2006) The metallogenesis of the Skorpion non sulphide zinc deposit, Namibia, 133 p. Ph. D .Thesis (Dr. rer. nat.), Mathematisch-naturwissenschaftlich-technischen Fakultät der Martin-Luther-Universität Halle-Wittenberg, Germany.

Kloprogge, T., Komarneni, S., and Amonette, J. (1999) Synthesis of smectite clay minerals: a critical review. Clays and Clay Minerals, 47, 529–554.

Large, D. (2001) The Geology of non-sulphide zinc deposits - an overview. Erzmetall, 54, 264–276.

Mellini, M., Nieto, F., Alvarez, F., and Gómez-Pugnaire, M.T. (1991) Mica-chlorite intermixing and altered chlorite from the Nevado-Filabride micaschists, Southern Spain. European Journal of Mineralogy, 3, 27–38.

Miranda-Trevino, J.C., and Coles, A.C. (2003) Kaolinite properties, structures and influence of metal retention on pH. Applied Clay Science, 23, 133–139.

Mondillo N., Boni M., Balassone G., Villa I.M. (2014a) The Yanque Prospect (Peru): form polymetallic Zn-Pb mineralization to a nonsulfide deposit. Economic Geology, 109, 1735–1762.

Mondillo N., Boni M., Balassone G., Villa I.G. (2014b) Polymetallic Zn-Pb mineralization in the Cuzco area (Peru): Lead isotope geochemistry Accha-Larisa district. Mineral Deposits Studies Group

552 Conference, Southampton, UK, 16-19 December 2014.

553 Newman, A.C.D., and Brown, G. (1987) The chemical constitution of clays. In Newman, A.C.D., Ed.,
554 Chemistry of Clays and Clay Minerals, Mineralogical Society Monograph, n. 6, p. 1–128, Wiley
555 Interscience, New York.

556 Nieto, F., and Livi, K.J.T. (2013) Minerals at the nanoscale. EMU Notes in Mineralogy, 14, 440 p.

557 Nieto, F., Ortega-Huertas, M., Peacor, D., and Arostegui, J. (1996) Evolution of illite/smectite from
558 early diagenesis through incipient metamorphism in sediments of the Basque-Cantabrian Basin.
559 Clays and Clay Minerals, 44, 304–323.

560 Pascua, C.S., Ohnuma, M., Matsushita, Y., Tamura, K., Yamada, H., Cuadros, J., and Ye, J. (2010)
561 Synthesis of monodisperse Zn-smectite. Applied Clay Science, 48, 55–59.

562 Peacor, D.R., Rouse, R.C., Bailey, S.W. (1988) Crystal structure of franklinfurnaceite: a tri-dioctahedral
563 zincosilicate intermediate between chlorite and mica. American Mineralogist, 73, 876–887.

564 Pecho, V., and Blanco, E.Z. (1983) Geología de los cuadrángulos de Chalhuanca, Antabamba y Santo
565 Tomás: Instituto de Geología, Minería y Metalurgia, Boletín, Lima, Peru, n. 35, 97 p.

566 Perelló, J., Carlotto, V., Zárate, A., Ramos, P., Posso, H., Neyra, C., Caballero, A., Fuster, N., and Muhr,
567 R. (2003) Porphyry-style alteration and mineralization of the Middle Eocene to Early Oligocene
568 Andauaylas-Yauri belt, Cuzco region, Peru. Economic Geology, 98, 1575–1605.

569 Petit, S., Righi, D., and Decarreau, A. (2008) Transformation of synthetic Zn-stevensite to Zn-talc
570 induced by the Hofmann-Klemen effect. Clays and Clay Minerals, 56, 645–654.

571 Robert, J.L., and Gaspérin, M. (1985) Crystal structure refinement of hendricksite, a Zn- and Mn-rich
572 trioctahedral potassium mica: a contribution to the crystal chemistry of Zinc-bearing minerals.
573 TMPM Tschermaks Mineralogische und Petrographische Mitteilungen, 34, 1–14.

574 Ross, C.S. (1946) Sauconite – a clay mineral of the montmorillonite group. American Mineralogist, 31,
575 411–424.

Roy, D.M., and Mumpton, F.A. (1956) Stability of minerals in the system ZnO-SiO_2-H_2O. Economic Geology, 51, 432–443.

Rule, A.C., and Radke, F. (1988) Baileychlore, the Zn end member of the trioctahedral chlorite series. American Mineralogist, 73, 135–139.

Srivastava, P., Singh, B., and Angove, M. (2005) Competitive adsorption behavior of heavy metals on kaolinite. Journal of Colloid and Interface Science, 290, 28–38.

Steinberg, M., Rautureau, M., Rivière, M. (1985) Analysis of zinciferous clays from central Tunisia using a scanning transmission electron microscope (STEM). Chemical Geology, 48, 157–164.

Tiller, K.G., and Pickering, J.G. (1974) The synthesis of zinc silicates at 20°C and atmospheric pressure. Clays and Clay Minerals, 22, 409–416.

Vazquez, M., Nieto, F., Morata, D., Droguett, B., Carrillo-Rosua, F.J., and Morales, S. (2014) Evolution of clay mineral assemblages in the Tinguiririca geothermal field, Andean Cordillera of central Chile: an XRD and HRTEM-AEM study. Journal of Volcanology and Geothermal Research, 282, 43–59.

Will, P., Friedrich, F., Hochleitner, R., Gilg, H.A. (2014) Fraipontite in the hydrothermally overprinted oxidation zone of the Preguiça mine, Southern Portugal. Abstract Mid-European Clay Conference, 16-19 September 2014, Dresden.

Zincore Metals, Inc. (2013) AZOD Zinc Oxide project, NI 43-101 Technical Report on a Preliminary Feasibility Study: Zincore Metals, Inc., Vancouver, Canada (http://www.zincoremetals.com/_shared/pdf/170848_Zincore_PFS_TechReport_AZOD_26August2013_Final.pdf).

FIGURE CAPTIONS

Figure 1. a) General geologic map of the Andahuaylas-Yauri metallogenic province (modified from

Perelló et al. 2003). b) Geologic map of the Yanque deposit area (modified from Mondillo et al. 2014a). c) Geologic map of the Accha deposit area (modified from Boni et al. 2009).

Figure 2. a) Compact clay packages (Sample YA-B). The grey part is the organic resin used to consolidate the sample before the preparation of the thin section. b) Porous clay aggregates (Sample YA-B). c, d) Smectite grains overgrown upon mica nuclei, forming a compact clay package (sample YA-D). By STEM-EDX spectrum, mica contains K as main interlayer cation, and Al as main occupant of the octahedral site. e) Spongy Fe-hydroxides (white arrow) in a porous clay aggregate (Sample YA-B). f) Rhombic Fe-hydroxides micro-grains (white arrows) in a porous clay aggregate (Sample YA-D).

Figure 3. a, b) HAADF image and chemical map of sample YA-B: Fe-hydroxides grew filling pores and covering PCA-type smectites.

Figure 4. a) Electron diffraction pattern of a compact smectite packet (Sample YA-B). b) Electron diffraction pattern of the smectite packet epitaxial over a mica grain shown in figure 2d (Sample YA-D).

Figure 5. Sample YA-D. a) Close up view of figure 2c: sauconite packets with lattice fringes spacing of 10-11 Å. b) Smectitic packets together with other that shows a random interstratification of smectite and mica with measured spacing of 20 Å and intermediate composition between those of smectite and mica. c) Smectite packet with alternating fringes at 13 and 10 Å. Sample YA-B. d) Compact smectite packet showing a two-dimensional fringe spacing of 11.6 and 4.5 Å. e) Compact smectite packet with lattice fringe spacing variable between 16 and 17 Å and wavy microfabric. f) Hematite associated with sauconite, showing mosaic-domain type texture.

Figure 6. HAADF image and chemical map (Zn and Al) of sample YA-B: sauconite (green) and beidellite (purple) compact clay packages and porous clay aggregates. The qualitative EDX sauconite spectrum is characterized by a Zn peak more intense than in the beidellite spectrum, instead characterized by a more intense Al peak.

Figure 7. Chemical compositions of clays from the Yanque and Accha deposits.

Figure 8. Octahedral chemical compositions of sauconite and beidellite on the Zn-Al^{VI}-Fe+Mg diagram.

634
635

TABLE 1. Zn-bearing clay minerals and other phyllosilicates.

Name	Ideal formulas*
Baileychlore	$(Zn,Fe^{2+},Al,Mg)_6(Si,Al)_4O_{10}(OH)_8$
Bannisterite	$KCa(Mn^{2+},Fe^{2+},Zn,Mg)_{20}(Si,Al)_{32}O_{76}(OH)_{16}\cdot 4–12H_2O$
Fraipontite	$(Zn,Al)_3(Si,Al)_2O_5(OH)_4$
Franklinfurnaceite	$Ca_2(Fe^{3+},Al)Mn^{3+}Mn^{2+}{}_3Zn_2Si_2O_{10}(OH)_8$
Hendricksite	$K(Zn,Mg,Mn^{2+})_3(Si_3Al)O_{10}(OH)_2$
Sauconite	$Na_{0.3}Zn_3(Si,Al)_4O_{10}(OH)_2\cdot 4H_2O$

* IMA accepted.

636

637

TABLE 2. XRD semi-quantitative analyses of Yanque and Accha samples selected for TEM study, after Boni et al. (2009) and Mondillo et al. (2014).

Drillcore	Latitude (Y)[1]	Longitude (X)[1]	Drillhole elevation (m.s.l.)	Sample depth from the top of the core (m)	Sample name	hemimorphite	smithsonite	Zn-smectite	chalcophanite	cerussite	quartz	K-feldspar	calcite	dolomite	illite	kaolinite	goethite
YA-01	8430548	815103	3562	1.5	YA-A	O	OO	OOO	-	-	OO	-	OO	OO	OO	O	O
YA-02	8430449	815202	3566	5.0	YA-B	OOO	-	OOO	-	-	OO	-	-	-	-	O	OO
YA-05	8430484	815297	3549	8.5	YA-C	OO	-	OOO	-	-	OOO	O	-	-	-	OO	-
YA-13	8430673	815099	3544	9.0	YA-D	OO	-	OOO	-	OO	OO	O	-	-	O	-	O
YA-20	8430461	815295	3553	9.0	YA-E	-	-	OOOO	O	-	OOO	O	-	-	-	O	-
MET1-26	8453672	186758	4287	98.5	ACC	-	O	OOOO	OOO	-	OOO	-	-	-	-	O	-

Note: [1]Coordinates: UTM, zone: 18L (Yanque) and 19L (Accha), datum: WGS84;

- not found, O <5 wt.%, OO 5-20 wt.%, OOO 20-40 wt. %, OOOO 40-60 wt. %

638

639

TABLE 3. Representative structural formulas (a.p.f.u.) of sauconite from Yanque and Accha deposits.

	YA-A	YA-A	YA-B	YA-C	YA-C	YA-D	YA-D	YA-E	ACC	ACC	ACC
Si	3.88	3.64	3.64	3.31	3.65	3.49	3.69	3.54	3.38	3.48	3.23
Al^{IV}	0.12	0.36	0.36	0.69	0.35	0.51	0.31	0.46	0.62	0.52	0.77
Al^{VI}	0.36	0.28	0.33	0.72	0.35	0.20	0.34	0.23	0.27	0.48	0.48
Mg	0.11	0.25	0.24	0.26	0.18	0.22	0.05	0.46	0.15	0.16	0.24
Fe^{2+}	0.13	-	0.15	0.31	0.04	0.18	0.18	0.13	0.20	-	0.09
Zn	1.97	2.34	2.29	1.43	2.18	2.37	2.24	2.08	2.28	2.07	2.02
Mn	0.18	0.00	-	0.02	0.04	-	-		-		
∑	2.75	2.87	3.01	2.74	2.78	2.97	2.82	2.89	2.90	2.71	2.84
K	0.05	0.05	0.09	0.27	0.07	0.07	0.07	0.05	0.04	0.18	-
Ca	0.11	0.14	0.21	0.11	0.18	0.15	0.13	0.20	0.26	0.22	0.31
∑ charge	0.27	0.34	0.51	0.49	0.43	0.37	0.33	0.46	0.55	0.62	0.62

Note: calculated based on 12 total anions, $O_{10}(OH)_2$

640

641

TABLE 4. Representative structural formulas (a.p.f.u.) of beidellite from the Yanque deposit.

	YA-A	YA-B	YA-B		YA-E	YA-E
Si	3.51	3.83	3.37	Si	3.62	3.37
Al^{IV}	0.49	0.17	0.63	Al^{IV}	0.38	0.63
Al^{VI}	1.65	1.49	1.46	Al^{VI}	2.00	2.01
Mg	0.14	0.14	-	Mg	-	
Fe^{3+}	0.17	0.29	0.26	Fe^{3+}	0.03	0.03
Zn	0.33	0.14	0.52	Zn	0.03	0.05
Mn	0.02	-	-	Mn	-	-
∑	2.31	2.06	2.24	∑	2.07	2.10
Na	-	-	-	Mg	0.09	0.12
K	0.05	0.16	0.14	K	0.02	0.03
Ca	-	0.05	0.14	Ca	-	0.05
∑ charge	0.05	0.26	0.42	∑ charge	0.19	0.38

Note: calculated based on 12 total anions, $O_{10}(OH)_2$

642

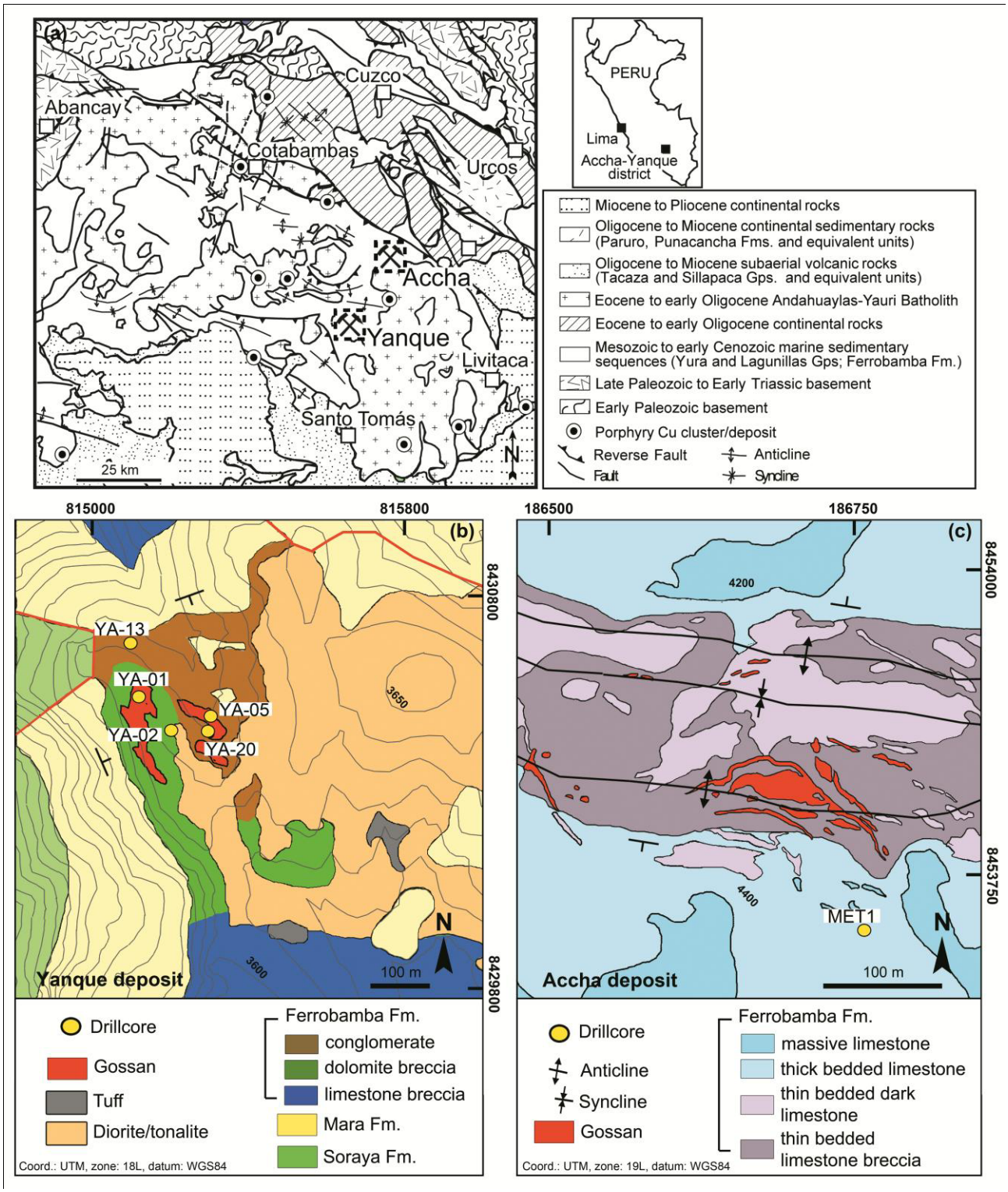
(a)
Cuzco
Abancay
Cotabambas
Urcos
Accha
Yanque
Livitaca
Santo Tomás
25 km
N
PERU
Lima
Accha-Yanque district
Miocene to Pliocene continental rocks
Oligocene to Miocene continental sedimentary rocks (Paruro, Punacancha Fms. and equivalent units)
Oligocene to Miocene subaerial volcanic rocks (Tacaza and Sillapaca Gps. and equivalent units)
Eocene to early Oligocene Andahuaylas-Yauri Batholith
Eocene to early Oligocene continental rocks
Mesozoic to early Cenozoic marine sedimentary sequences (Yura and Lagunillas Gps; Ferrobamba Fm.)
Late Paleozoic to Early Triassic basement
Early Paleozoic basement
Porphyry Cu cluster/deposit
Reverse Fault
Fault
Anticline
Syncline
815000
815800
(b)
8430800
8429800
YA-13
YA-01
YA-05
YA-02
YA-20
3650
3600
N
100 m
Yanque deposit
Drillcore
Gossan
Tuff
Diorite/tonalite
Ferrobamba Fm.
conglomerate
dolomite breccia
limestone breccia
Mara Fm.
Soraya Fm.
Coord.: UTM, zone: 18L, datum: WGS84
186500
186750
(c)
8454000
8453750
4200
4400
MET1
N
100 m
Accha deposit
Drillcore
Anticline
Syncline
Gossan
Ferrobamba Fm.
massive limestone
thick bedded limestone
thin bedded dark limestone
thin bedded limestone breccia
Coord.: UTM, zone: 19L, datum: WGS84

Figure 1

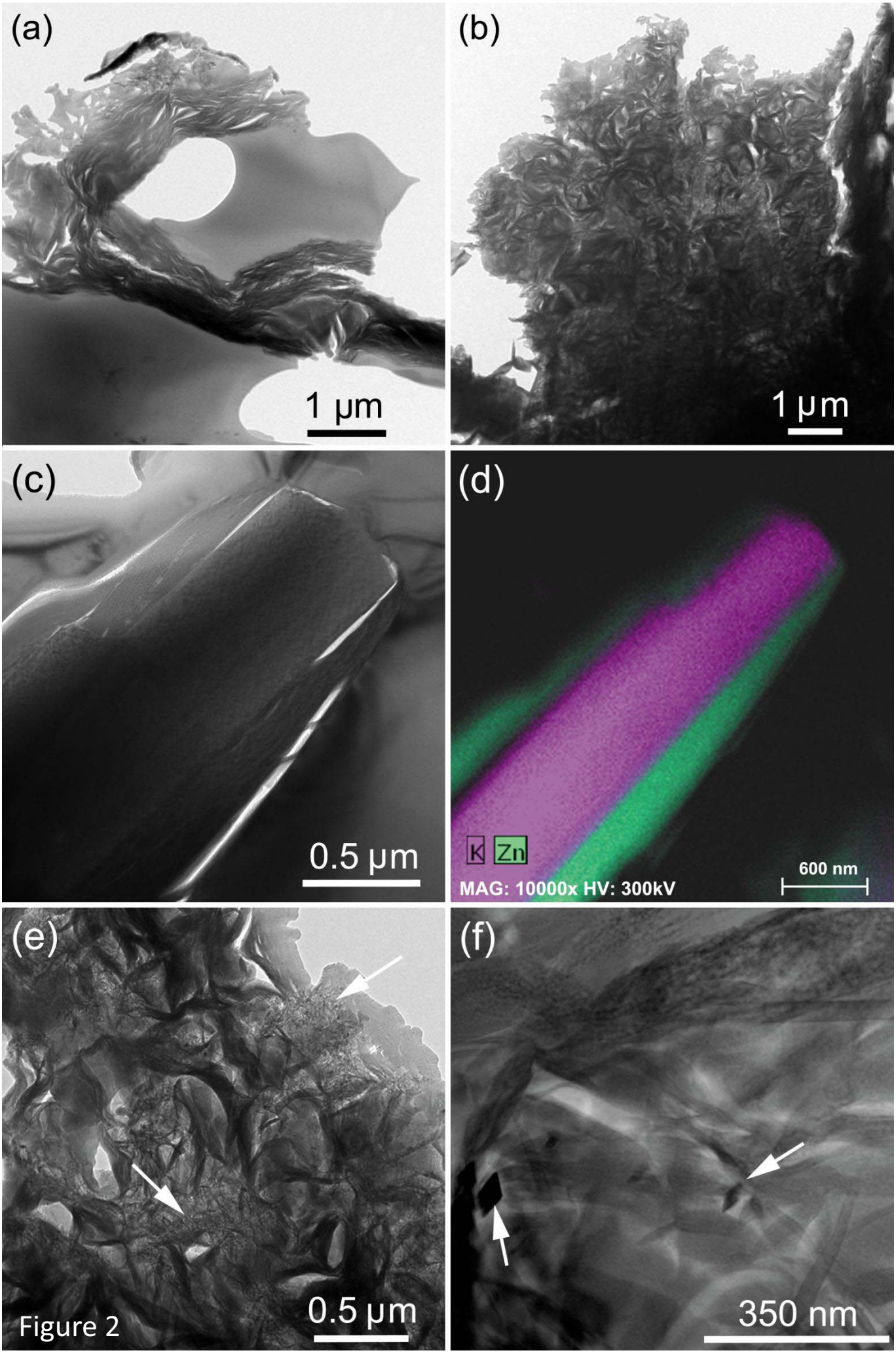

Figure 2

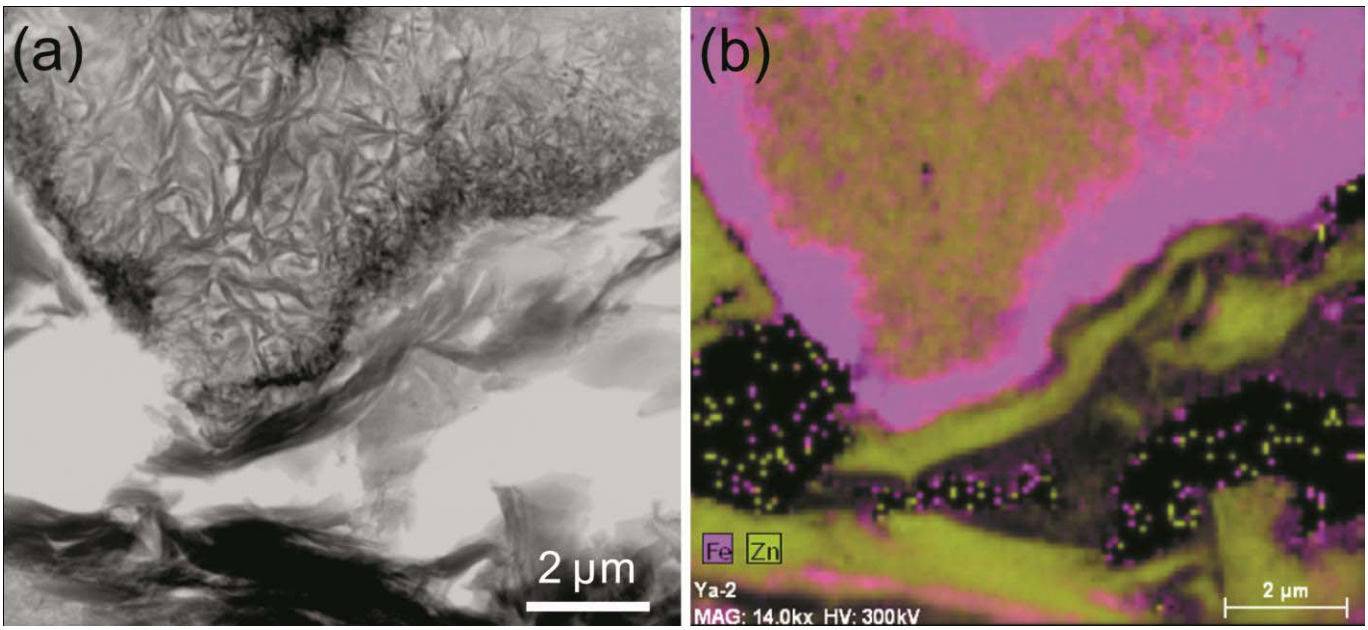

Figure 3

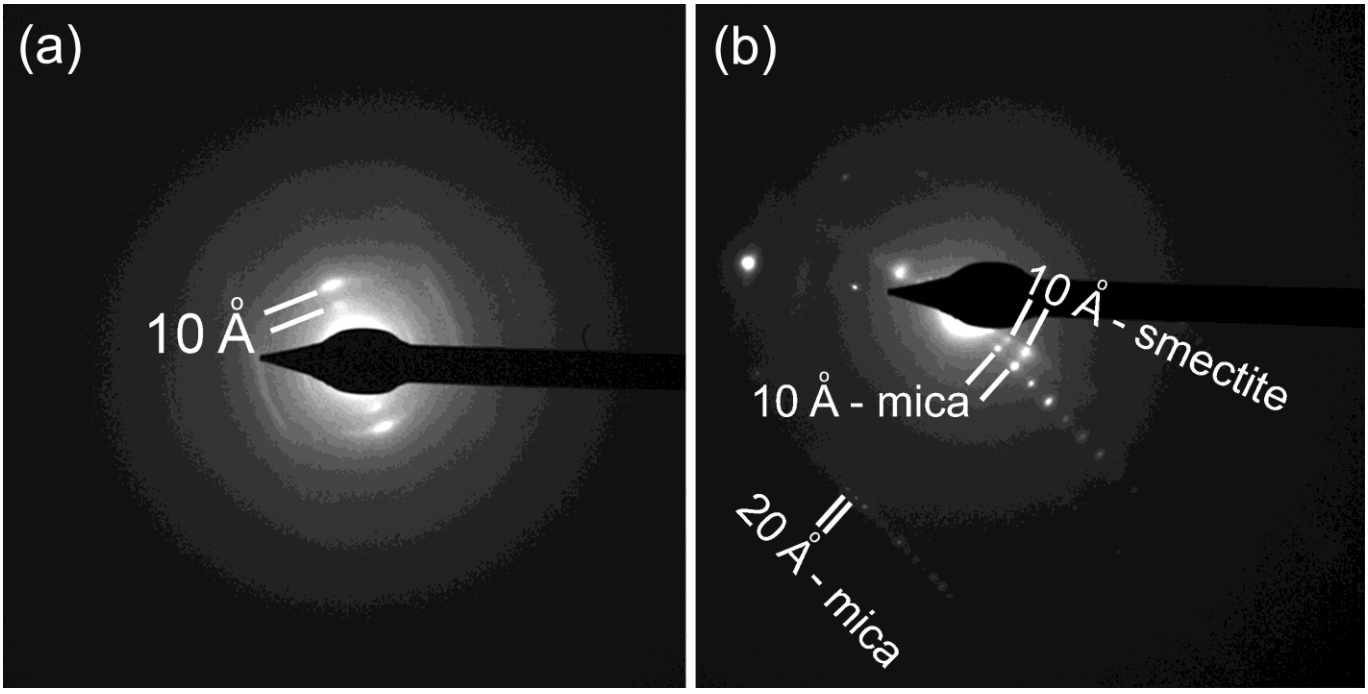

Figure 4

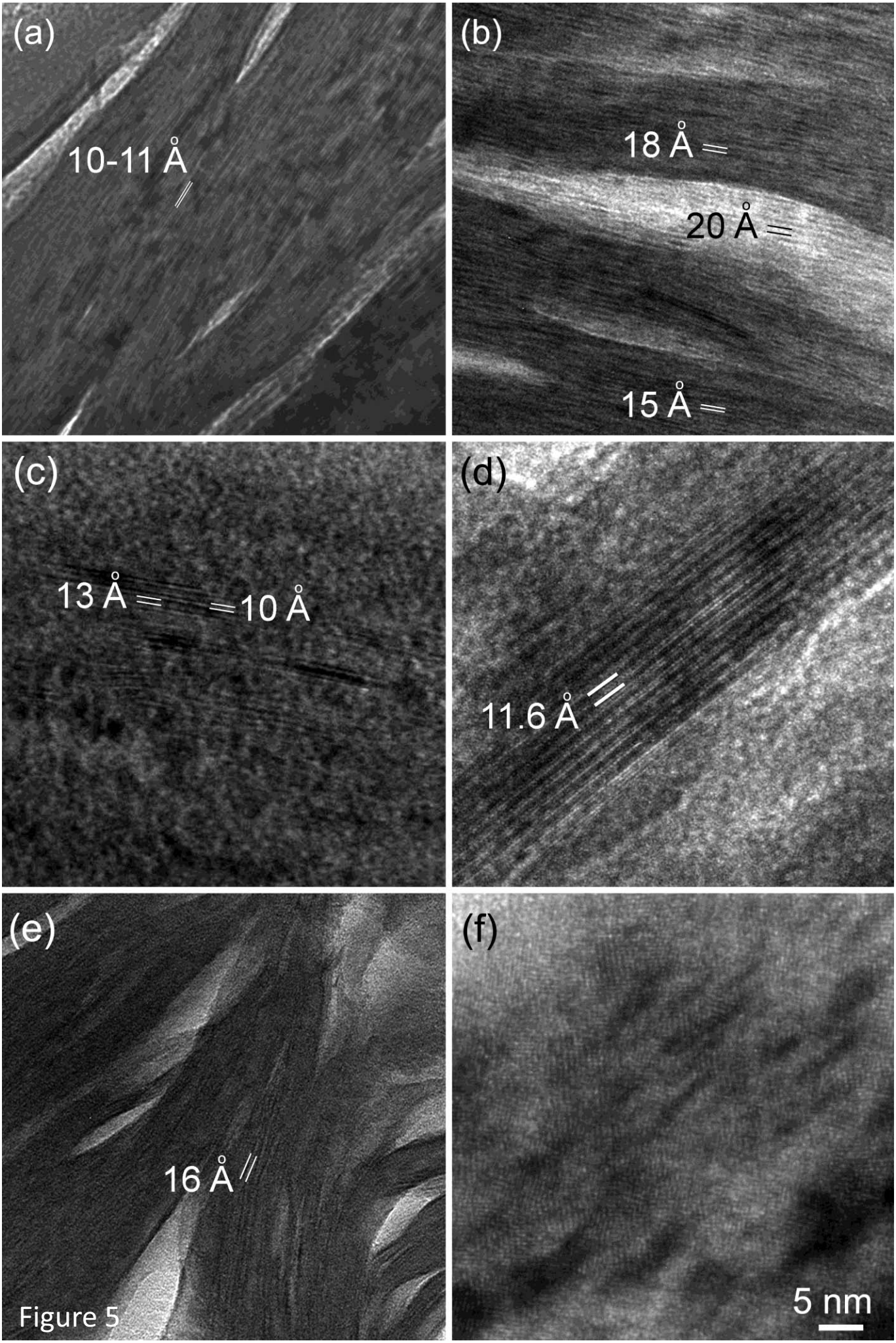

Figure 5

Figure 6

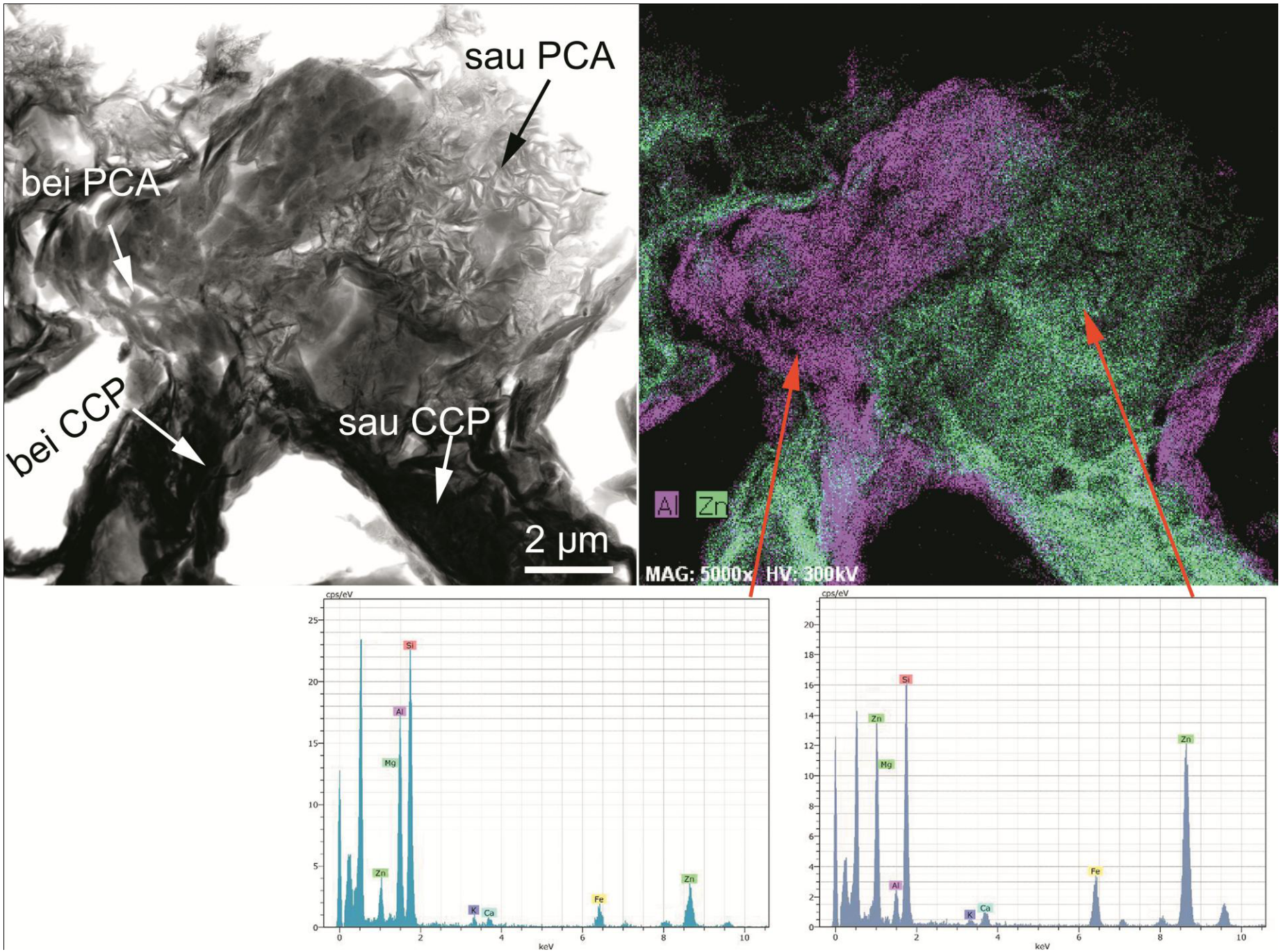
sau PCA
bei PCA
bei CCP
sau CCP
2 µm
Al
Zn
MAG: 5000x HV: 300kV
cps/eV
Si
Al
Mg
Zn
K
Ca
Fe
Zn
keV
cps/eV
Si
Zn
Mg
Al
K
Ca
Fe
Zn
keV

Figure 7

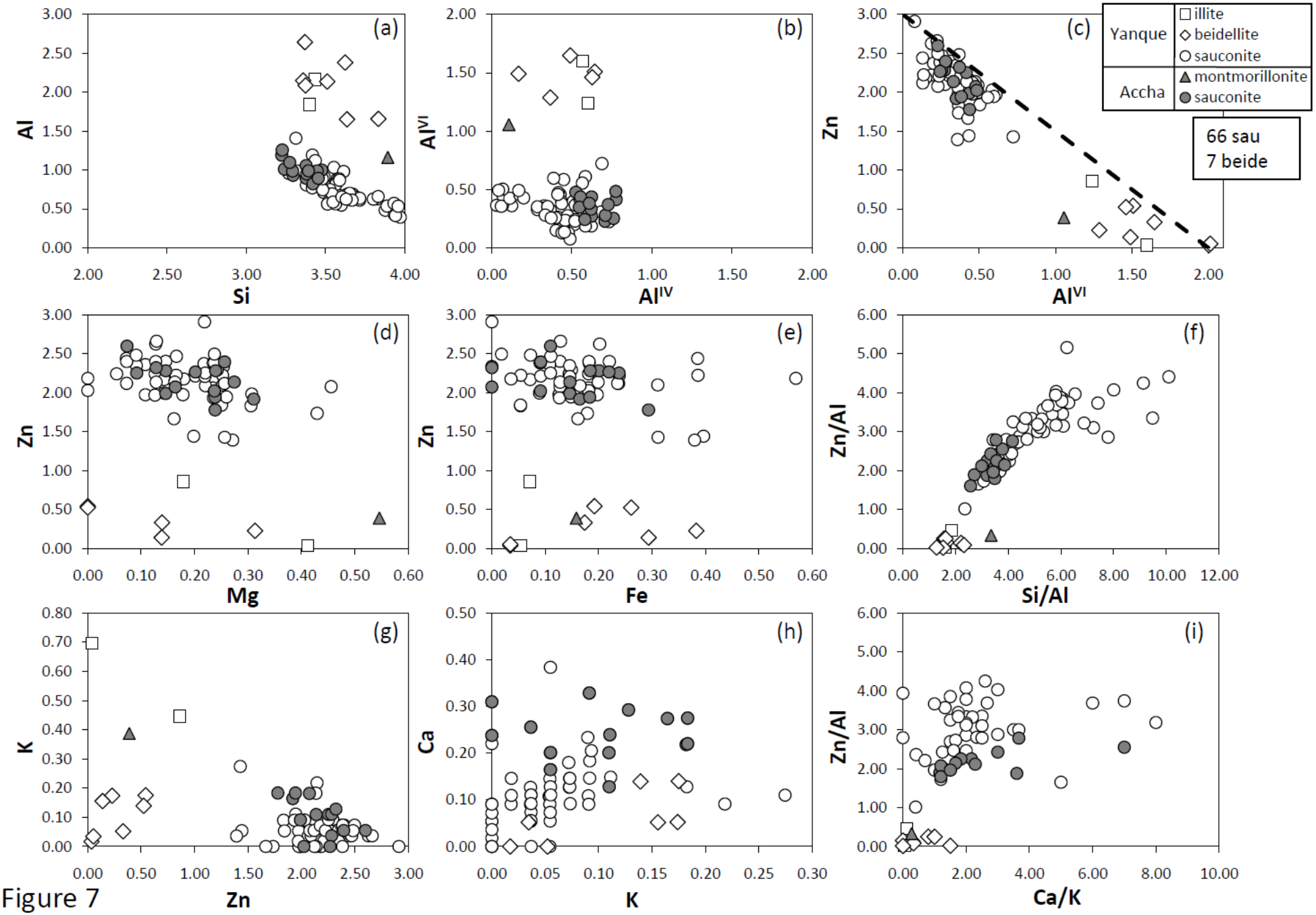

Figure 7

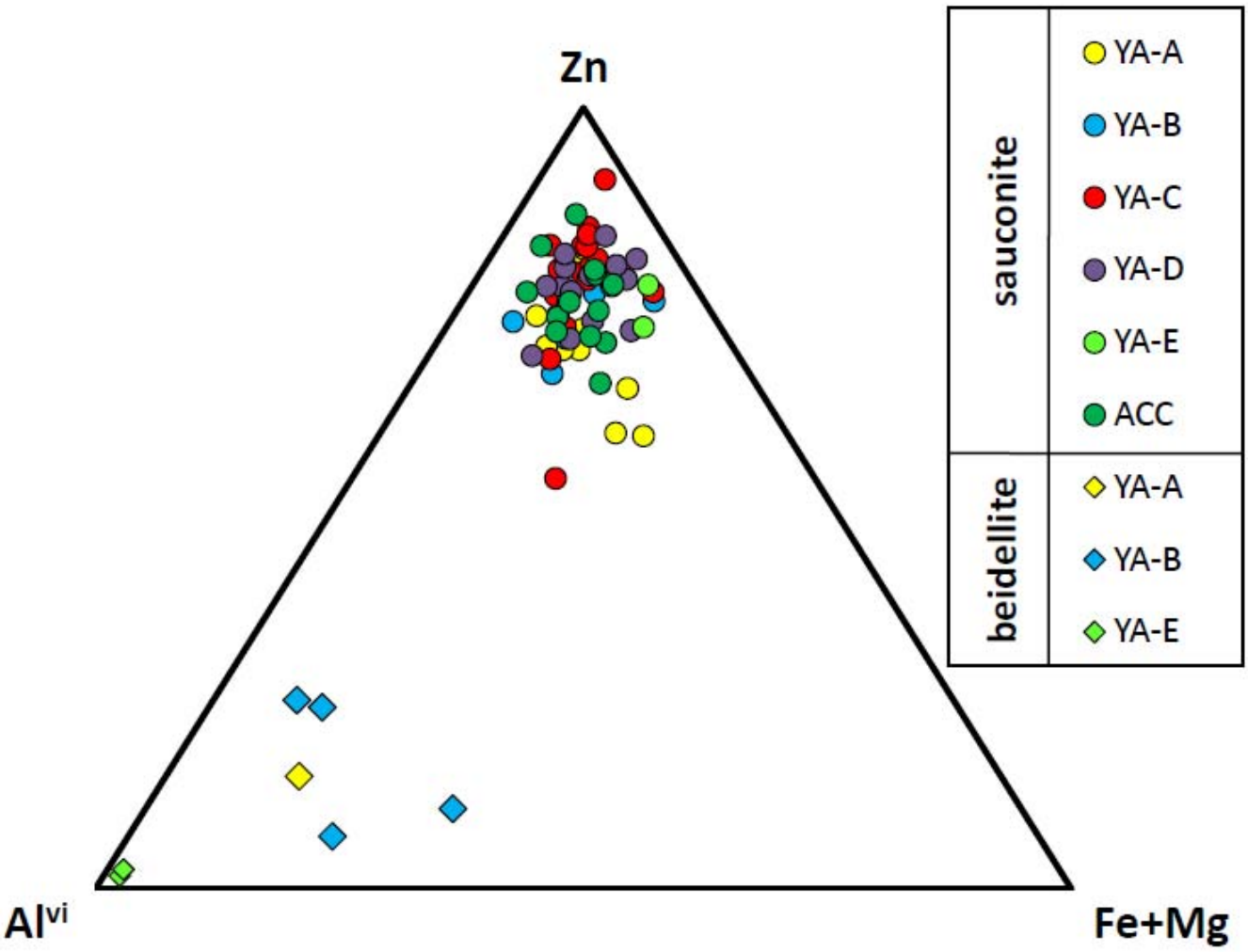
Zn
Al^vi
Fe+Mg
sauconite
YA-A
YA-B
YA-C
YA-D
YA-E
ACC
beidellite
YA-A
YA-B
YA-E

Figure 8